doi: 10.1016/j.eurpolymj.2022.111169

Design of cysteine-S-sulfonated keratin via pH driven processes: Micro-Structural Properties, Biocidal Activity and *in vitro* Validation

Diego O. Sanchez Ramirez[a]*, *Cinzia Tonetti*[a], *Iriczalli Cruz-Maya*[b], *Vincenzo Guarino*[b], *Roberta Peila*[a], *Riccardo A. Carletto*[a], *Alessio Varesano*[a] *and Claudia Vineis*[a]

[a]CNR-STIIMA (National Research Council - Institute of Intelligent Industrial Technologies and Systems for Advanced Manufacturing), Corso Giuseppe Pella 16, 13900 Biella, Italy

[b]CNR-IPCB (National Research Council - Institute for Polymers, Composites and Biomaterials), Mostra d'Oltremare, Pad. 20, V.le J.F. Kennedy 54, 80125 Napoli, Italy

*corresponding author:
E-mail address: diegoosr@hotmail.com

Abstract

Cysteine-S-sulfonated keratin, protein extracted from wool fibers by sulfitolysis, is a natural polyelectrolyte typically used in biomedical materials like scaffolds and smart biointerfaces. In order to extend and tune its properties, a study of the content of secondary structures, thermostability, biocidal activity and *in vitro* tests of cell viability on lyophilized cysteine-S-sulfonated keratin were carried out as a function of the pH solution (after keratin extraction and before purification). The results offer considerable evidence of the formation of protein-ligand complexes due to the protonation of keratin, with the presence of bisulfite, citrate, formate and acetate ions. These interactions modify the content of secondary structures in cysteine-S-sulfonated keratin, increase its thermostability (~50°C), enhance the stability of positive charges that confers its biocidal activity ($pH_{solution}$<5.2) and change the interaction between cysteine-S-sulfonated keratin and human mesenchymal stem cells. Lastly, *in vitro* and antibacterial tests confirm that pH changes may also influence cell and bacteria response, in terms of proliferation, due to the changes of protein secondary structure and positive/negative charges. These results give relevant insights into the process of tuning keratin properties for biomedical applications – i.e., drug delivery, wound healing.

Keywords: keratin, biocidal protein, thermostability, cell viability, protein-ligand complexes

1. Introduction

Polyelectrolytes are polymers that contain ionizable groups in their structure. This type of polymers has demonstrated many applications which depend on their charge, concentration, pH, etc. [1-4]. Polyelectrolytes can be synthesized or extracted from natural sources [4-6]. Natural polyelectrolytes have shown a lot of potential thanks to their biocompatibility [1,3,4]. Furthermore, it is well known that the protonation/deprotonation of polyelectrolytes can influence the growth/adhesion of cells and bacteria [7,8]. For example, chitosan and alginate have been widely used as natural sources of polycations and polyanions [1,4]. Nevertheless, other natural polyelectrolytes, like proteins, have a great potential to exploit: collagen, casein and keratin are the most popular among them. In particular, the latter can be extracted from many natural sources such as horns, feathers, hair and animal fibers [9,10].

Keratin is a valuable biopolymer that has multiple ionizable side chains. These contain a variety of functional groups that permit the adsorption of ions (heavy metals and dyes) from aqueous solutions [11-13]. This protein can be extracted from wool fibers by the reduction, oxidation or sulfitolysis of their disulfide bonds which produce kerateine (cysteine residues), keratose (cysteic acid residues) or cysteine-S-sulfonated keratin (cysteine and cysteine-S-sulfate residues), respectively. In particular, the latter is obtained thanks to the presence of sodium dodecyl sulfate as a surfactant, urea as a denaturing agent of hydrogen bonds and sodium metabisulfite as a reducing agent of disulfide bonds [14,15].

Keratin is made of intermediate filament proteins, which are mainly classified into keratin type I (acid family – pI between 4.75 and 5.4) and keratin type II (neutral-basic family – pI between 5.4 and 6.7) [16]. Additionally, different isoelectric points (pI) have been found and demonstrated for these keratin types during separation processes in two-dimensional gel electrophoresis [16-18]. Consequently, the titration of these protein types could have underlying effects on the stability/properties and the separation of cysteine-S-sulfonated keratin during its purification process.

In fact, the importance of pH on stimuli-responsive keratin materials like hydrogels [19-21] and nanoparticles [22-24] for biomedical and drug-delivery applications has already been demonstrated in the literature. Nevertheless, the effect of pH on cysteine-S-sulfonated keratin during its protonation/deprotonation still needs to be investigated, as this kind of variations during keratin processing not only modify the adsorption of ions but also alter protein properties, for instance, biocidal activity and cell-material interactions. In particular, the former could have great potentiality as currently a spread of bacteria with antibiotic resistance (i.e. *Staphylococcus aureus*) generates a great concern around the world [25,26]. Likewise, its applications to prevent bacterial infections and enhance cell viability in burn wounds are very promising [27].

This work aims to assess the effect of varying pH values of keratin-solutions (before dialysis and after extraction) on the properties of cysteine-S-sulfonated keratin by studying the pH of the solution, the content of secondary structure and the thermal properties of lyophilized cysteine-S-sulfonated keratin. In addition, in order to extend the applications of this polyelectrolyte, a study of the biocidal activity and the cell viability on the resulting biomaterials has been carried out.

2. Materials and methods

2.1. Materials

All reagents were purchased from Sigma Aldrich unless otherwise indicated: sodium metabisulfite (CAS 7681-57-4), sodium dodecyl sulfate (CAS 151-21-3), urea (CAS 57-13-6), NaOH (CAS 1310-73-2), HCl (CAS 7647-01-0), citric acid (CAS 77-92-9), formic acid (CAS 64-18-6), acetic acid (CAS 64-19-7), DL-dithiothreitol (CAS 3483-12-3), tris(hydroxymethyl)amino-methane (CAS 77-86-1), thiourea (CAS 62-56-6), Bovine Serum Albumin (CAS 9048-46-8).

Petroleum ether 40 - 60 °C RPE for analysis (CAS 64742-49-0, Carlo Erba Reagents) was used in a soxhlet extractor for 2 h to degrease carded white fibers from wool. After that, fibers

were wrung out and the solvent was evaporated in a chemical fume hood. Fibers were successively scoured in deionized water for 1 h at room temperature and for 1 h at 50 °C. Finally, fibers were dried in an oven for 4 h at 50 °C and stored for 24 h at 20 °C and 65 %RH.

2.2. Keratin Extraction and Titration

The extraction of cysteine-S-sulfonated keratin from fibers was carried out by using a solution of sodium metabisulfite 0.6 M, urea 8.0 M and sodium dodecyl sulfate 0.07 M. The pH value and temperature of extraction were set at 6.5 (with NaOH 5 M) and 65 °C; the extraction time was 2 h and 30 min, as it is reported in the literature [14]. Afterward the solution was filtered and all titrations were done in a conditioned environment at 20 °C. About 20 ml of the extraction solution with cysteine-S-sulfonated keratin were titrated up to a pH value above 6.5 (7.0, 7.5 and 8.0) and below the value of 6.5 (6.0, 5.5, 5.0, 4.5, 4.0 and 3.5). The solutions having a pH above the value of 6.5 were prepared by the addition of NaOH 5 M, while the pH values below 6.5 were achieved by the addition of different acid solutions (citric acid 3.6 N, formic acid 13.3 N, acetic acid 8.7 N and HCl 6.0 N). Citric, formic and acetic acids were included in acid titrations as these weak acids can be employed in the processing of cysteine-S-sulfonated keratin powders (in particular formic acid). The addition of acid/basic solutions was done by using manual Transferpette® (Single-channel from BrandTech®). Finally, solutions after pH adjustment and prior to dialysis were kept at room temperature for at least 2 h.

The final solutions, with cysteine-S-sulfonated keratin at different pH, were purified by using dialysis tubing cellulose membrane (molecular weight cutoff 14000 Da). Dialysis were carried out in 800 ml of deionized water (pH 5.63 ± 0.16 and conductivity 6.5 ± 2.8 µS cm^{-1}) for 3 days in a conditioned environment at 20 °C. Every day the deionized water was changed at least 3 times and its pH and conductivity were measured, through a Pc 8 Instrumental Bench (pH/mV/COND/TDS/°C) – Carli Biotec equipped with a polymer electrode for pH and a conductivity electrode (VPT 51/01 for a range between 0.1 µS cm^{-1} and 1 mS cm^{-1} –

Standards solutions: 5, 500 and 1413 µS cm^{-1}). Moreover, the variation of conductivity over time (µS cm^{-1} h^{-1}) was calculated with every measure to verify the state of the purification process of cysteine-S-sulfonated keratin. The dialysis was stopped when the variation of conductivity was below 0.30 µS cm^{-1} h^{-1} (Table S1).

The solutions of purified cysteine-S-sulfonated keratin were filtered in vacuum with a qualitative filter paper (Whatman® grade 1, pore size 11 µm) to separate the insoluble fraction generated during dialysis; pH, conductivity and volume of these solutions were measured. After that, the solutions were frozen (– 28 °C) and lyophilized for 7 days in a Heto PowerDry PL3000 Freeze Dryer at – 55 °C and 23 hPa. The protein concentration in solution ($g_{protein}$ mL^{-1}) was calculated using the weight of lyophilized cysteine-S-sulfonated keratin and the volume of solution. Then, a definition analogous to molar conductivity (mS cm^2 mol^{-1}) was used to identify the electrical behavior of this polyelectrolyte in solution and verify the reproducibility of lyophilized cysteine-S-sulfonated keratin produced at different pH values – it was defined as the specific conductance (Λ_s) of solution (mS cm^2 $g_{protein}^{-1}$) and calculated dividing the conductivity of solution after filtration (mS cm^{-1}) by the concentration of protein ($g_{protein}$ cm^{-3}). Every test and measurement for each acid/alkali titration were conducted twice.

2.3. Electrophoresis

One-dimensional electrophoreses in Invitrogen NuPAGE 7% Tris-acetated gels of 1.5 mm × 15 wells (36 to 500 kDa separation range) were done in an XCell SureLock Mini-Cell Electrophoresis system (Invitrogen). Before electrophoresis, lyophilized samples of cysteine-S-sulfonated keratin were solubilized at 16 mg protein mL^{-1} in a buffer solution of pH 8.5 (25 mM Tris base, 2.4 M thiourea, 5 M urea and 5 %wt. dithiothreitol). Then, the Bio-Rad Protein Assay (Bradford method) was employed using the protein concentration calibration curve of Bovine Serum Albumin to confirm the real concentration of protein without humidity content. Successively, a solution of 3.0 µg protein $µL^{-1}$ was prepared (from solution of 16 mg protein mL^{-1}) following the buffer preparation for Denaturing Electrophoresis in NuPAGE Technical

Guide - Reduced Sample. Finally, electrophoresis were run with the suitable running buffer (NuPAGE Tris-acetate SDS - 20x from Invitrogen) at 200 V. The Coomassie Blue-R staining was used to stain the proteins.

2.4. FT-IR Analysis

The spectrums of lyophilized cysteine-S-sulfonated keratin were recorded from 4000 to 650 cm^{-1} with 100 scans and 4 cm^{-1} band resolution, by a Thermo Nicolet Nexus spectrometer with an ATR accessory - Smart Endurance (diamond crystal ZnSe focusing element). All spectrums were normalized at 1645 cm^{-1} (amide I peak).

The secondary structure quantification of cysteine-S-sulfonated keratin samples was carried out by fitting the Amide I peak with Gaussians. For all spectrums a baseline correction was employed between Amide I and Amide II peaks. The wavenumber of each secondary structure was determined by means of the second derivate method using the quadratic Savitzky-Golay smoothing (third-order polynomial with five points). The frequency of secondary structures was assigned as follows: intermolecular β-sheets 1611, 1618, 1625 and 1695 cm^{-1} [28-30], intramolecular β-sheets 1674 cm^{-1} [31], the bands between 1630 and 1640 cm^{-1} can be assigned to inter and/or intramolecular β-sheets [31,32] and were called "β-sheets II" to express the effect of bands in this region, β-turns 1668, 1682 and 1689 cm^{-1} [29,30], α-helix 1645, 1651, 1659 cm^{-1} [33-35], random coil 1645, 1651 and 1659 cm^{-1} [33,34]. Furthermore, the small bands contributions due to side-chain (1594 and 1604 cm^{-1}) and carboxylic groups adsorptions (1714, 1725 and 1731 cm^{-1}) were also considered [33,36,37], but the quantification of secondary structures was carried out excluding those areas. All data were analyzed by using the function peak analyzer of OriginPro 2015. As reported in the literature, the fitting of Amide I peak was carried out limiting the values of Full Width at Half Maximum (FWHM) between 10 and 30 cm^{-1}, allowing any positive value for the height of

Gaussians and fixing the band position [33]. The estimation for each acid/alkali titration was conducted twice.

2.5. Differential Scanning Calorimetry (DSC) Analysis

DSC analysis were performed by using a Mettler Toledo DSC from 30 to 500 °C with a heating rate of 10 °C min^{-1}. The calorimeter cell was flushed with 100 mL min^{-1} of nitrogen and the mass of every sample of cysteine-S-sulfonated keratin powder was ~1.0 mg. This test was conducted twice for each acid/alkali titration.

2.6. Antibacterial Tests

For every test, the ASTM E2149-2013 "Standard test method for determining the antimicrobial activity of antimicrobial agents under dynamic contact conditions" Test Method was used employing the Gram-positive *Staphylococcus aureus* ATCC 6538. The incubated test culture in a nutrient broth was diluted in a buffer (pH 7.0) to give a concentration of 1.5–3.0 × 10^5 CFU mL^{-1} (working dilution). Each sample was transferred to flask containing a volume of the working solution at the ratio 50 mL:1 g. All flasks were shaken for 2 h at 190 rpm. After a series of dilutions, 1 mL of the solution was plated in nutrient agar. The inoculated plates were incubated at 37 °C for 24 h and surviving cells were counted. The antimicrobial activity was expressed in percent reduction of the organisms after contact with the test specimen compared to the number of bacterial cells surviving after contact with the control, according to Equation 1:

$$Reduction\ (\%) = (B - A)/B \times 100 \quad (1)$$

where A is CFU mL^{-1} after contact (end test) and B is CFU mL^{-1} at zero contact time. Antibacterial test for each acid/alkali titration was conducted twice.

2.7. Cell culture tests

For these tests, 50 mg of lyophilized cysteine-S-sulfonated keratin were compressed with 10 ton press to produce protein pellets of 13 mm diameter and 0.3 mm thickness using a manual hydraulic press. The selected samples were sterilized with ethanol (≥99.8 %) for 24 h.

Human mesenchymal stem cells (hMSCs, SCC034 from Sigma-Aldrich, Milan, Italy) were used for *in vitro* tests. Firstly, hMSCs were cultured in a 75 cm^2 cell culture flask in Eagle's alpha minimum essential medium (α-MEM) supplemented with 10% fetal bovine serum (Sigma-Aldrich, Milan, Italy), antibiotic solution (streptomycin 100 µg mL^{-1} and penicillin 100 U mL^{-1}, Sigma-Aldrich, Milan, Italy) and 2mM of L-glutamine, incubated at 37 °C in a humidified atmosphere with 5% CO_2 and 95% air. hMSCs from 5-6 passage were used for cell proliferation assays. Before cell culture, samples were cut and put in a 96-well culture plate, then rinsed with PBS and dried under hood. hMSCs were seeded at 5×10^4 to perform proliferation assays using cell counting kit-8 reagent (CCK-8; Dojindo Laboratories) at 1, 3 and 7 days. Cell culture media was removed and changed. At each time point by 100 µL of fresh medium with 10 µL of CCk-8 reagent per well and incubated 4 hours in standard conditions. The supernatant was collected, and absorbance was measured at 450 nm using a microplate reader.

3. Results and discussion

3.1. Properties of cysteine-S-sulfonated keratin solution – pH and Λs

As far as titrations are concerned, it is important to remember that the extraction solution has a considerable amount of chaotropic agent (urea) and surfactant (sodium dodecyl sulfate), which induce an unfolded structure in proteins [38,39]. It facilitates not only the protonation of side-chains but also modifies the solvation shell of cysteine-S-sulfonated keratin due to the presence of sulfite ions, citric acid, formic acid, acetic acid and their dissociated forms. During the dialysis process, the concentrations of chaotropic agent and surfactant are reduced allowing the protein refolding. Nevertheless, sulfite ions, citric acid, formic acid, acetic acid and their dissociated forms are ligands and these could remain bound to the protein. For more information about these ligands and their interactions with other proteins, visit the Protein Data Bank. Consequently, the formation of protein-ligand complexes between bisulfite ions/weak acids in dissociated forms and cysteine-S-sulfonated keratin is possible.

It is necessary to highlight that even though acid/alkali titrations included the isoelectric points of keratin type I (acid family – pI between 4.75 and 5.4) and keratin type II (neutral-basic family – pI between 5.4 and 6.7), these underwent a coagulation without complete flocculation (Figure S1). The presence of surfactant (sodium dodecyl sulfate), chaotropic agent (urea) and ionic species (Na^+, Cl^-, H^+, OH^-, bisulfite, citrate, formate or acetate) prevent cysteine-S-sulfonated keratin from a complete flocculation during its titration. The flocculation and precipitation of proteins take place mainly during dialysis when species different from cysteine-S-sulfonated keratin are removed from solution. The aggregation of cysteine-S-sulfonated keratin takes place because of the fact that the majority of electrostatic repulsion disappear. However, the presence of charges in this polyelectrolyte and the formation of protein-ligand complexes improve the stability of cysteine-S-sulfonated keratin in solution and prevent its complete precipitation under the experimental conditions studied in this work.

pH measurements before and after dialysis for every titration are reported in Figure S2 (in this figure boxes labelled $R_{i=1,..,5}$ are used to indicate samples with similar pH values after dialysis). The experimental data were fitted by linear/nonlinear regressions and the results are reported in Table S2 and Figure S2 (the pI ranges for keratin type I and II were also included). The results of citric acid, formic acid and acetic acid can be represented by the logistic function dose-response in pharmacology/chemistry. In comparison with HCl, the deviation from linearity is likely due to weak acids bound to cysteine-S-sulfonated keratin. These results show that those protein-ligand complexes have the property to act as a buffer protein system and this capacity can be considerably enhanced by weak acids, mainly acetic acid. The pH in acid titrations confirms that H^+ ions have protonated cysteine-S-sulfonated keratin and its protonated state can be kept in aqueous solutions after dialysis, as described by the Gibbs-Donnan effect [40-42].

Additionally, it is possible to say that the affinity of ligands (sulfite ions, citric acid, formic acid, acetic acid and their dissociated) towards the protonated cysteine-S-sulfonated keratin allowed the formation of protein-ligand complexes. This affinity was increased and decreased by the reduction and the growth of pH, respectively. This means that this affinity was better when compounds with negative charges (acetate, citrate, formate and sulfite ions) were employed during acid titrations. The strong interactions between the positive charges of polypeptide chains and the negative charges of anions are the main cause of the formation of buffer protein system (in solution) and proteins-ligand complexes (in lyophilized powder). The latter can also manifest pH memory after freeze-drying, as reported in the literature for other proteins [43,44]. All subsequent pH should be henceforth treated as the pH values after the dialysis process, unless otherwise indicated.

All Λ_s measurements are reported in Figure S3. When the pH before dialysis was at the pI of keratin type I, a minimal value was reached in titrations done with carboxylic acids. The minimal for HCl was found almost at the same point. At its pI, the net electrical charge of cysteine-S-sulfonated keratin in aqueous solution was neutral and its capacity of binding additional ions (Cl^-, OH^-, bisulfite, citrate, formate or acetate) and transporting charges was minimal as well. Above and below the pI of keratin type I, the average value of Λ_s tended to increase even with a similar pH value after dialysis (see R_1–R_5 in Figure S3). Furthermore, R3 (pH 4.50 and pH 4.75) can be considered the region where the precipitation of keratin occurs due to its pI. Therefore, cysteine-S-sulfonated keratin could undergo variations in its composition below R3.

Also, a considerably increase of standard deviation for pH values after dialysis (Figure S2) and for Λ_s values was observed (Figure S3) when acid titrations with HCl and formic acid were below the pI of keratin type I. In citric acid and acetic acid cases, the standard deviations were smaller than in the other two acids cases. It is necessary to highlight that a greater value of standard deviation increases the possibility of obtaining heterogeneous cysteine-S-

sulfonated keratin which could cause variability in its properties. This is the reason why all reported properties will be studied in the following sections.

3.2.Qualitative characterization of lyophilized cysteine-S-sulfonated keratin

The results of one-dimensional gel electrophoresis are reported in Figure 1. All lyophilized keratin samples titrated above and below pH 6.5 showed the same bands of cysteine-S-sulfonated keratin without pH variations (see pH 6.5 lines). These results are in accordance with the literature [16-18]. Therefore, it can be assumed that pH treatments kept approximately stable the molecular weight of cysteine-S-sulfonated keratin even below R3.

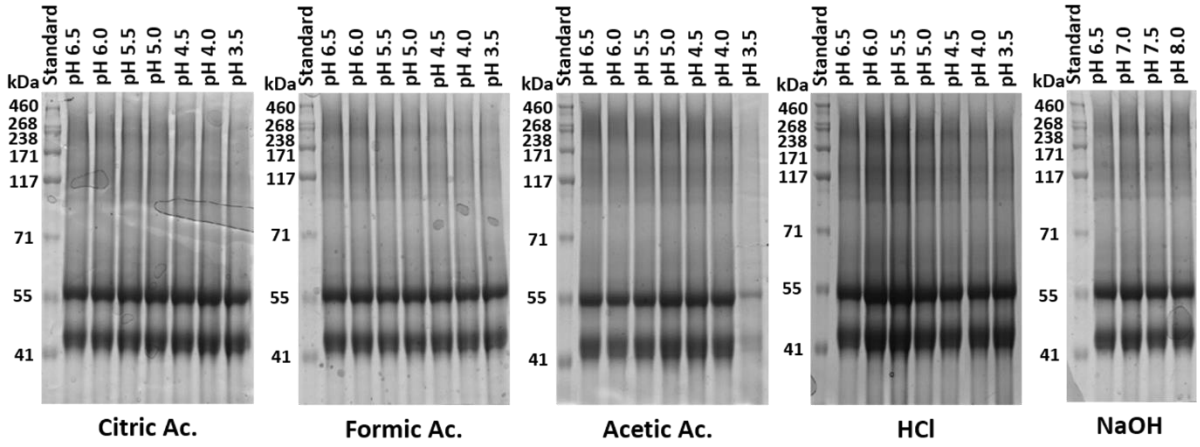

Figure 1. Electrophoresis for lyophilized cysteine-S-sulfonated keratin for each acid/basic titration (the pH values correspond to titration values). pH 6.5 lines refer to a sample without pH variation.

On the other hand, it was qualitatively observed that freeze-dried cysteine-S-sulfonated keratin that came from alkali titrations produced a sponge-like compact structure, while those originated from acid titrations tended to form powders at low pH values, Figure S4. However, all keratin samples after freeze-drying showed a similar flake form without additional variations when examined by electron microscopy, Figure S4. These differences confirmed the effect of pH on the mechanical properties of keratin materials, as reported in the literature [19,20]. As a result, the structural differences of lyophilized cysteine-S-sulfonated keratin are driven by the carboxylate group ($R–COO^-$), whose amount increases during alkali titrations [19,20]. It induces the formation of expanded structures during the freezing and crystallization

of cysteine-S-sulfonated keratin in solution, which in turn results in sponges instead of powders after lyophilization.

3.3. Conformational properties of lyophilized cysteine-S-sulfonated keratin

All FT-IR spectrums and the content of secondary structures are reported in Figure S2-S7 and Figure 2-3, respectively. In terms of intermolecular β−sheet structures, it can be seen that pH modifications by acids (citric acid, formic acid, acetic acid and HCl) tend to increase the percentage of this structure, while NaOH induces reductions with a rise of standard deviations. As mentioned above, the content of intermolecular β−sheet is given by bands at 1611, 1618, 1625 and 1695 cm^{-1} [28-30]; however, the bands at 1625 and 1695 cm^{-1} are probably the main responsible for the increase of intermolecular β−sheet conformation, as these are associated to interactions among separate proteins that cause aggregation processes [28,32].

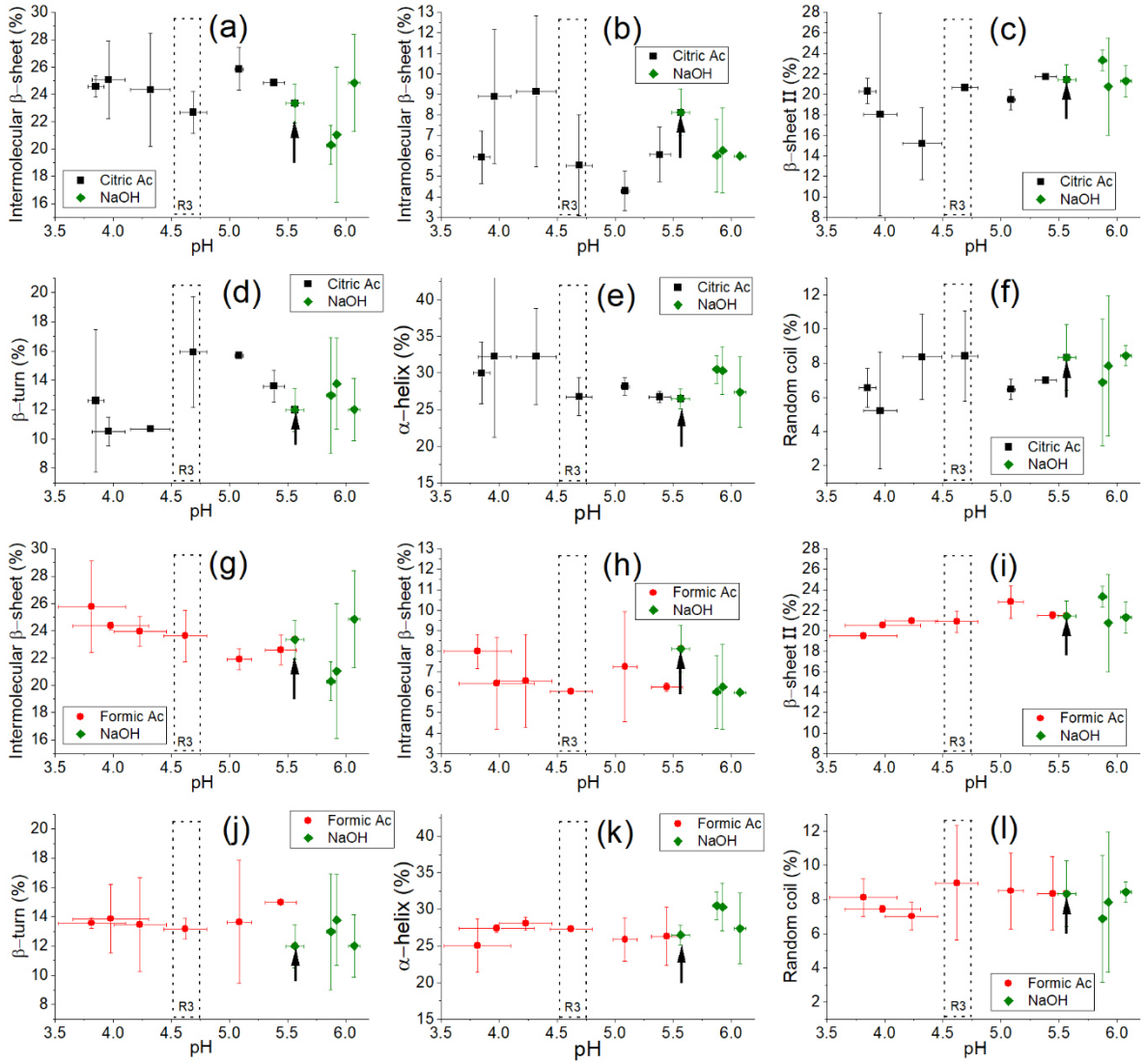

Figure 2. Secondary structures content of cysteine-S-sulfonated keratin from citric (a – f) and formic (g – l) acid titrations. The arrow indicates the sample without addition of acids or alkali.

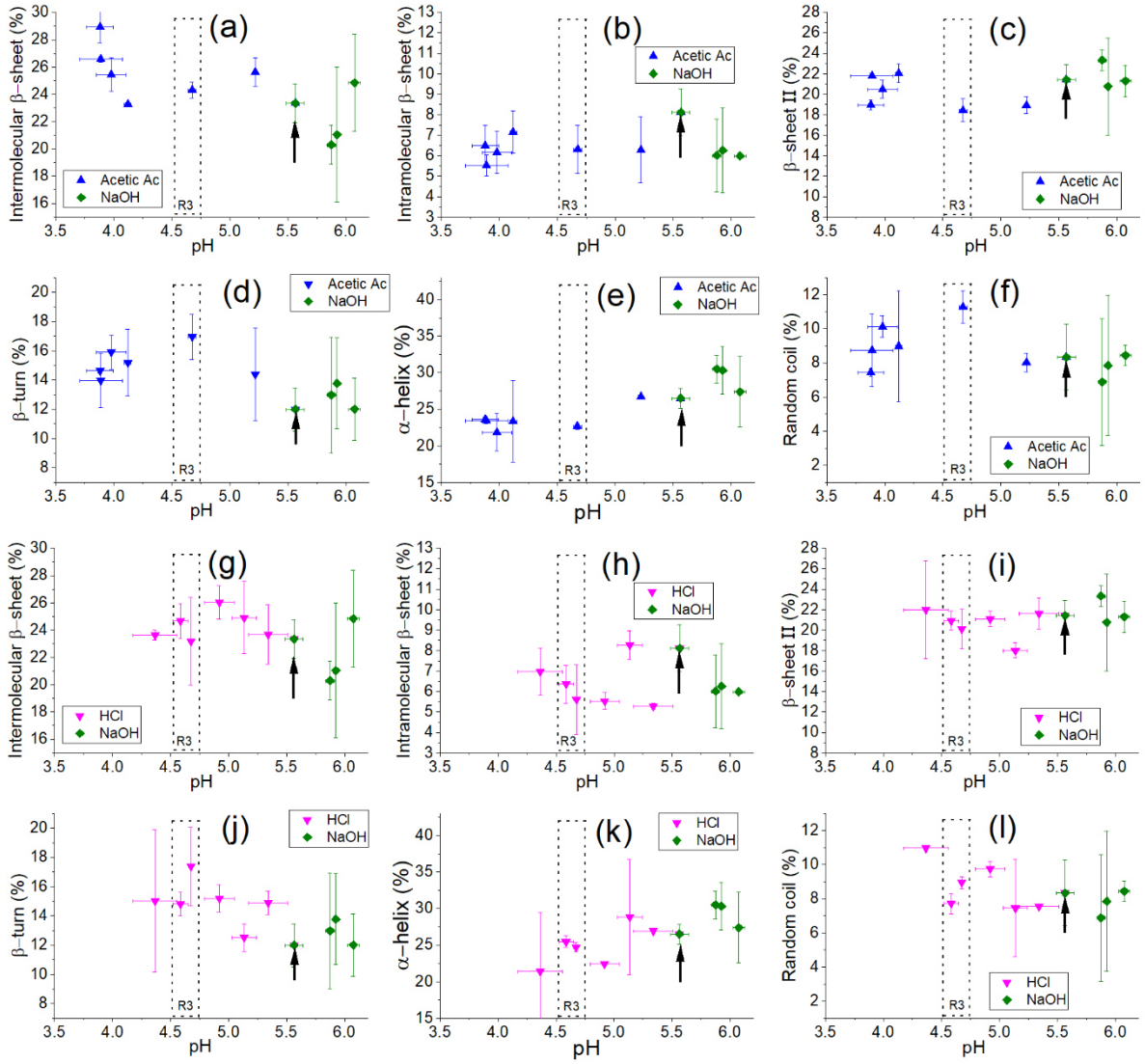

Figure 3. Secondary structures content of cysteine-S-sulfonated keratin from acetic acid (a – f) and HCl (g – l) titrations. The arrow indicates the sample without addition of acids or alkali.

As regards intramolecular β–sheet, small reductions are induced by acetic acid and formic acid compared to HCl and citric acid, where the two latter have shown a sharp drop and a steep growth of this type of conformation, in particular for HCl above R3. β–sheet II contributions for HCl and citric acid had similar variations before R3; after that, these structures drops in citric acid case with an increase of standard deviations. The changes of β–sheet II for formic acid were minimal, while acetic acid has shown a slight fall up to R3. In NaOH, a reduction is noticed for intramolecular β–sheet conformations and for β–sheet II contributions variations were neglected.

On the other hand, β–turn structures reported a growth up to R3 with a subsequent decrease for all samples obtained from acids, excepting formic acid that had its increase at pH 5.3. A tendency to decrease or keep stable α–helix conformation was observed for acetic acid, formic acid and HCl. In contrast, citric acid displayed an increase after R3, but standard deviation rose as well. In literature, it has been reported that compounds with a great capacity to generate hydrogen bonds (citric acid and hexafluoroisopropanol) can raise the content of α–helix structures in cysteine-S-sulfonated keratin [45,46]. NaOH showed also a slight increase of α–helix structures. In terms of random coil, the content of this structure tended to rise by reducing pH and the only exception was citric acid, whose content decreased (before R3).

The contributions of carboxylic groups above 1700 cm^{-1}, on the fitting of amide I peak, are reported in Figure 4 (a-d). These contributions are associated with the protonation of carboxylic groups (R–COOH) [15,47,48] and confirmed the addition of H^+ ions in cysteine-S-sulfonated keratin structure by the side-chains of amino acids (glutamic and aspartic acid). All acids stepped up the content of protonated R–COOH while NaOH reduced it, as expected. Furthermore, a maximum at pH 4.7 was observed with HCl and for any other acid a maximum was reached at pH 4.25, as Figure 4 (a-d) shows. The differences between HCl and weak acids are probably due to acid traces (citrate, formate and acetate ions). Moreover, when NaOH was employed, the stretching band of carboxylate group at 1397-1405 cm^{-1} was also detected [49,50], Figure 4 (e). The presence of this band involved the formation of $R–COO^-$ and the deprotonation of glutamic/aspartic acid in cysteine-S-sulfonated keratin structure after alkali titrations, which confirmed the assumption made in Section 3.2 and demonstrated the effect of $R–COO^-$ groups on the mechanical properties of cysteine-S-sulfonated keratin.

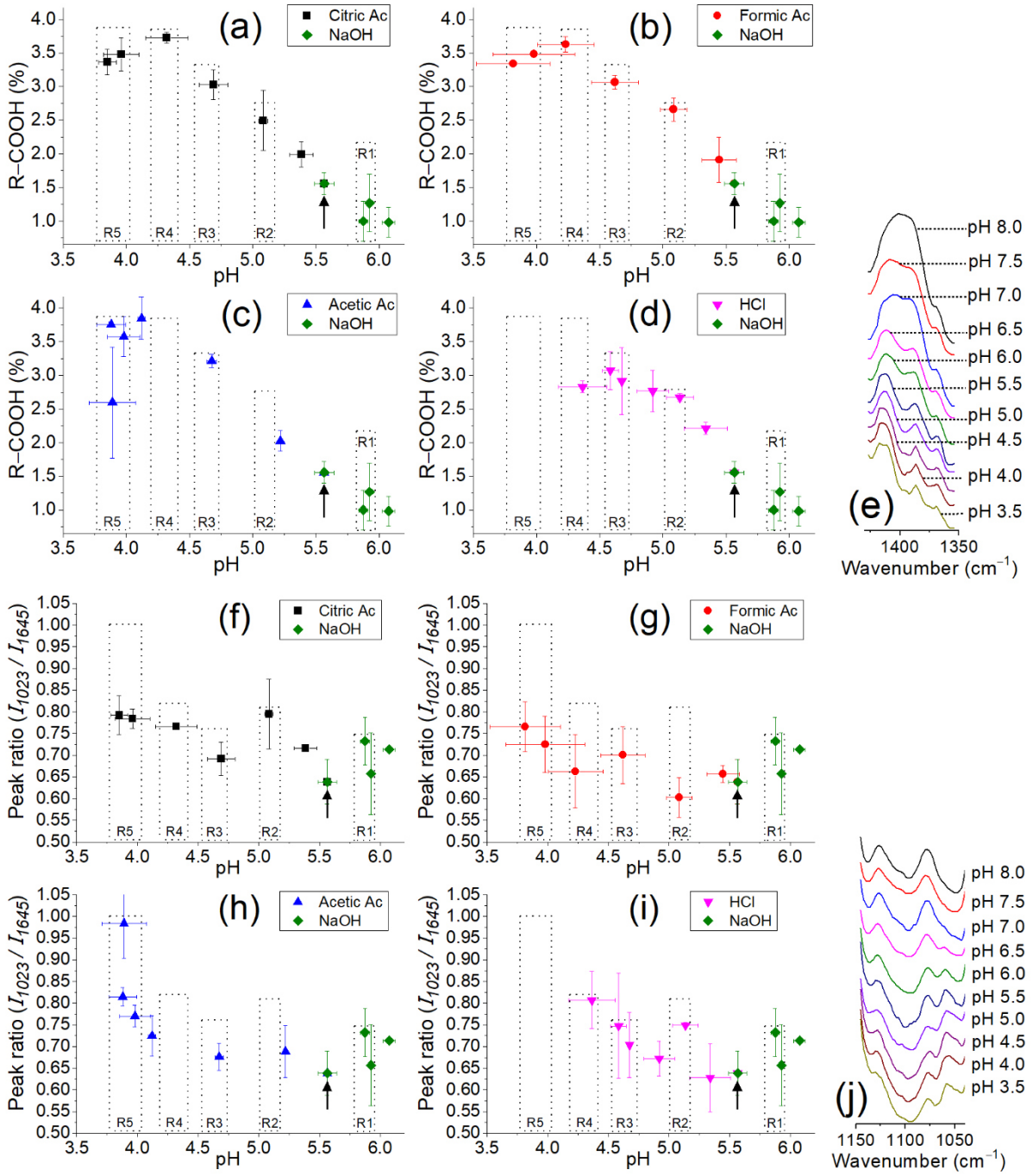

Figure 4. (a – d) Percentage of R–COOH in amide I peak, (e) R–COO$^-$ peak in FT-IR spectra, (f – i) peak ratio I_{1023}/I_{1645} and (j) bisulfite peaks between 1050-1150cm^{-1} in FT-IR spectra. The arrow in (a – d) and (f – i) indicates the sample without addition of acids/alkali. pH values on (e) and (j) correspond to titrations values.

Changes in the intensity of amide III (1200 cm^{-1}) and Bunte's salt residues (1023 cm^{-1}) were also seen (Figure S7). For this reason, the peak ratio of Bunte's salt residues/amide I (I_{1023}/I_{1645}) is reported in Figure 4 (f – i), the peak ratio of amide III/amide I showed similar results, Figure S8. Additionally, a new and small peak at 1057 cm^{-1} was also noticed when pH

was reduced, Figure 4 (j). The presence of this band and the variations of intensity in amide III (1200 cm^{-1}) and Bunte's salt residues peaks (1023 cm^{-1}) are probably a consequence of bisulfite ions that have been bound to cysteine-S-sulfonated keratin. In particular, $HOSO_2^-$ or its tautomeric form HSO_3^- report in literature vibrations at: 1030-1023 cm^{-1} for SO_3 symmetrical stretching in HSO_3^-, 1050 cm^{-1} for SO_2 symmetrical stretching in $HOSO_2^-$, 1128-1120 for S-H bending in HSO_3^-, 1196-1180 cm^{-1} for SO_3 asymmetrical stretching in HSO_3^-, 1200 for cm^{-1} S–O stretching in $HOSO_2^-$ [51,52]. All these results give considerable evidence of the presence of bisulfite ions and show that the intensity in amide III (or Bunte's salts) is also influenced by bisulfite ions ($HOSO_2^-$ or its tautomeric form HSO_3^-). It is worth remembering that amide III peak is a complex band also associated with the side-chains and hydrogen bonds of proteins [53-56]. Nevertheless, in the current work, the changes of intensity in amide III (or Bunte's salts) are probably a consequence of variations in the amounts of bisulfite ions.

Figure 4 (f – i) show that alkali titrations induce slight variations in comparison with acid titrations. It is due to the fact that the negative charges of deprotonated cysteine-S-sulfonated keratin prevent the adsorption of bisulfite ions and, analogously, the positive charges of protonated cysteine-S-sulfonated keratin enhance the adsorption of acetate, citrate, formate and bisulfite ions. Finally, it can be seen in Figure 4 (f – i) that all acid titrations had a convergent point at R3 that is probably caused by passing the pI of keratin type I.

As far as FT-IR results are concerned, it is possible to say that the variations of pH and the adsorption of ions can set the content of secondary structure in cysteine-S-sulfonated keratin. It gives rise to the formation of protein-ligand complexes, which keep their structures through hydrogen bonds and salt bridges [57]. The changes of these interactions among proteins can even modify the mechanical properties of lyophilized cysteine-S-sulfonated keratin, as seen in Section 3.2.

3.4. Thermal properties of lyophilized cysteine-S-sulfonated keratin

The thermal properties of cysteine-S-sulfonated keratin were studied and the results of the endothermic peak of denaturation are shown in the Figure S9. Figure 5 reports the variations of the endothermic heat and temperature of cysteine-S-sulfonated keratin denaturation at different pH values. This peak tended to diminish its endothermic heat (area under the peak) with pH reduction, Figure 5 (a). In the literature, this peak is associated with the crystallites of α–helix [58,59]. Therefore, its reduction could represent a decrease in the content of this structure when pH is reduced and its increase could express a growth of α–helix crystallites during alkali titrations. Figure 2 and 3 confirms these assumptions, as α–helix content underwent a slight increase in alkali titrations and a reduction in acid titrations. However, it is important to highlight that the endothermic heat of denaturation is heavily influenced by the presence of pyrolysis reactions when the temperature is above 200 °C [45, 60-62].

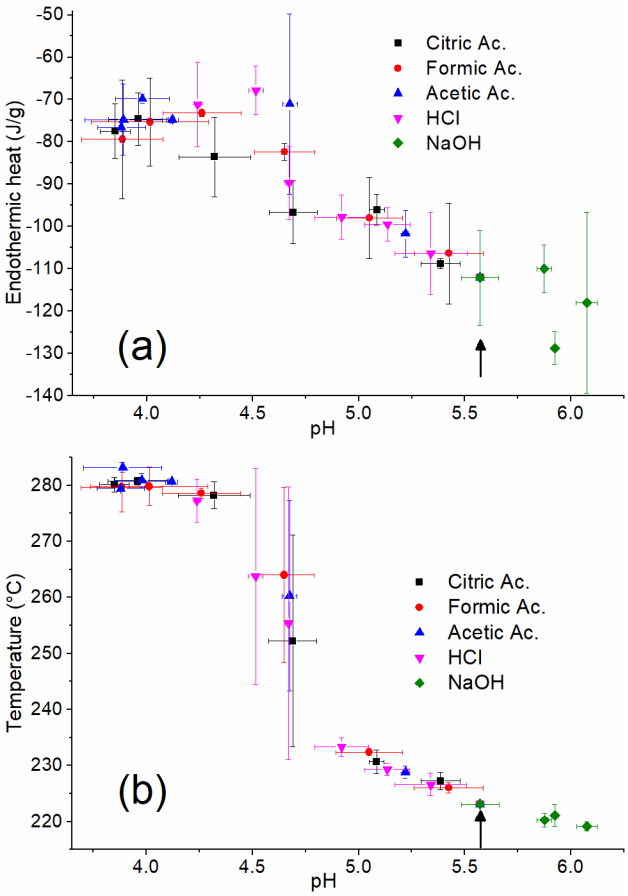

Figure 5. Endothermic heat (a) and temperature (b) for the denaturation peak of cysteine-S-sulfonated keratin. The arrow indicates the sample without the addition of acids or alkali.

Figure 5 (b) shows the temperature of the endothermic peak: the temperatures increased when the pH value was reduced and slightly decreased when the pH value stepped up. A transition zone was found between 4.75 and 4.50 (R3) caused by the pI of keratin type I. All acid titrations showed a considerable increase in the temperature of the denaturation peak (~50 °C), particularly for pH values below 4.5. Similar results have been reported in the literature for hair treated at different pH values [60]. These results could originate from the raise of intermolecular β–sheet structures (as seen in Figure 2 and 3), as the formation of more aligned chains involves an increase of crystallinity and a rise of melting temperature [63,64]. As a result, intermolecular β–sheet structures contribute to enhance the thermostability of α–helix crystallites in cysteine-S-sulfonated keratin from acid titrations.

Finally, it can be said that the increasing thermostability of proteins is a well-known consequence of protein-ligand interactions. It usually happens thanks to hydrogen bonds, hydrophobic interactions and salt bridges between ligands and proteins [65,66]. In this work, an increase of hydrogen bonds and a strong electrostatic interaction between the protonated structure of cysteine-S-sulfonated keratin and anionic ligands (bisulfite, citrate, formate and acetate ions) contribute to the formation of more aligned intermolecular β–sheet structures which causes an increasing thermostability in lyophilized cysteine-S-sulfonated keratin during acid titrations. Therefore, the increase of denaturation temperature is due to the energy required to remove anionic ligands from protein chains before its irreversible unfolding process happens [65]. To summarize, a schematic representation of cysteine-S-sulfonated keratin-ligand complexes from acid and alkali titrations has been reported in Schema S1.

3.5. Antibacterial properties of lyophilized cysteine-S-sulfonated keratin

The biocidal activity of cysteine-S-sulfonated keratin samples was studied against *S. aureus*. It is well known that polymers with positive charges can kill bacteria by destabilizing their negatively charged membrane [67]. Therefore, these tests were employed to quantify the antibacterial action of cysteine-S-sulfonated keratin-ligand complexes for potential applications and indirectly confirm the protonation of these samples. The results for samples without modification and for those resulting from acid titrations are reported in Figure 6. This figure shows that all samples demonstrated a complete antibacterial activity when the pH was below ~5.25. That is to say, pH 5.25 corresponds to the point where the protonation effect becomes significant for antibacterial applications. Below this pH, the protonation of cysteine-S-sulfonated keratin tends to increase until the saturation of H^+ ions on side-chains groups, as seen in Figure 4.

As regards the presence of bisulfite, citrate, formate and acetate ions and their possible effects on the biocidal activity of protonated cysteine-S-sulfonated keratin, it is relevant to remember that metabisulfite ions ($S_2O_5^{2-}{}_{(aq)}$) in aqueous solutions form different species ($HSO_3^-{}_{(aq)}$, $HOSO_2^-{}_{(aq)}$, $SO_3^{2-}{}_{(aq)}$, $SO_{2(g)}$ and $H^+{}_{(aq)}$) in equilibrium. The presence and concentration of each species depend heavily on the pH value of solution [68-70]. Indeed, the dynamic equilibrium of those ions is the main cause of antimicrobial protection in wines due to the release of $SO_{2(g)}$ at pH < 4.0, as this gas can diffuse through the cell membrane of microorganisms and disrupt their metabolism [71-73]. The dominant form in this dynamic equilibrium (pH 3.5 – pH 6.5) is bisulfite ion ($HSO_3^-{}_{(aq)}$ and $HOSO_2^-{}_{(aq)}$), that is to say, a reducing agent that prevents the oxidation of compounds and keeps the organoleptic properties of foods and beverages.

In HCl case, the pH value of solutions after dialysis was always above 4.0 (see Figure S2 and S3) and, consequently, the release of $SO_{2(g)}$ was not possible. Moreover, considering the fact that antibacterial tests were carried out in a buffer at pH 7.0 during a contact time of 2 h, the

formation and diffusion of $SO_{2(g)}$ inside the bacteria were excluded. Considering all this information, it is possible to assume that a bacterial reduction of 100 % for pH values below 5.25 in HCl case (Figure 6) can be attributed to the positive charges of cysteine-S-sulfonated keratin. Finally, the bisulfite ions bound to this polyelectrolyte might enhance the conservation of this protein and prevent its oxidation over time.

As seen in Figure 4, lyophilized cysteine-S-sulfonated keratin in acid titrations showed a slight increase of peak intensity above 1700 cm^{-1}. Indeed, the content of R–COOH grew up to about 3.0 % and 3.75 % for HCl and weak organic acids (citric, formic and acetic acid), respectively. It demonstrated that the amount of carboxylic acids bound to protein chains was below 1%. These weak organic acids were likely bound in their dissociated forms (anions) and a pH 7.0 during antibacterial tests kept these forms. Furthermore, it is important to mention that the main mechanism of action to kill bacteria by weak organic acids entails the diffusion of their undissociated forms through the negatively charged membrane of bacteria to alter its intracellular pH and/or membrane function [27,74,75]. Therefore, the possibility that anionic forms of these acids could have any effect on the biocidal activity of protonated cysteine-S-sulfonated keratin can be excluded.

As the antibacterial activity of all cysteine-S-sulfonated keratin samples was tested in a buffer at pH 7.0 during a contact time of 2 h, it is possible to say that the protonation state and the pH memory of cysteine-S-sulfonated keratin-ligand complexes were kept. The pH memory is a consequence of a strong affinity between protonated cysteine-S-sulfonated keratin and anionic ligands. This affinity creates strong ties, which prevents other molecular bindings, with greater concentration than anionic ligands but lower affinity, affecting cysteine-S-sulfonated keratin properties [76]. In the light of this result, the biocidal activity of these complexes is not considerably affected by pH - especially in the case of samples obtained from acid titration with a pH value below 5.25.

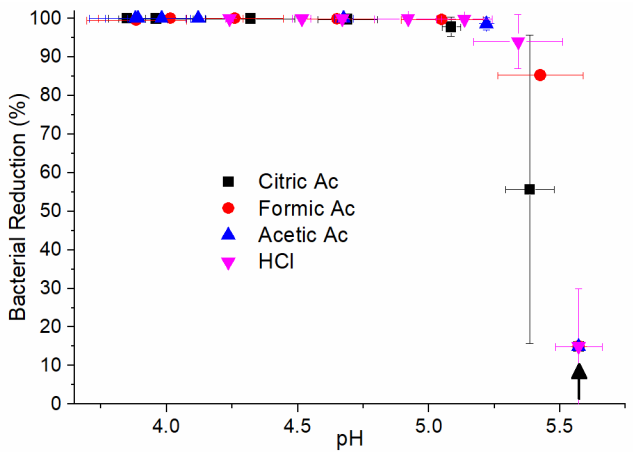

Figure 6. Bacterial reduction against *S. aureus* of cysteine-S-sulfonated keratin powder. The arrow indicates the sample without addition of acids or alkali

On the contrary, a growth of *S. aureus* colonies was noticed when the bacteria were brought into contact with samples from alkali titrations (Figure 7, upper row) which confirmed the absence of positive charges. Similar behavior was observed for cysteine-S-sulfonated keratin samples aged up to three years (Figure 7, lower row). Aged cysteine-S-sulfonated keratin was stored in a container with air at 20 °C and 65% HR. Alkali titrations demonstrated to be a good method to accelerate the aging process of cysteine-S-sulfonated keratin. Therefore, the aging process of cysteine-S-sulfonated keratin is accompanied by an increase of negative charges on its structure. On the other hand, it is worth mentioning that *S. aureus* can produce different types of extracellular enzymes like deoxyribonuclease, lysozyme, lipase and proteinase [77,78]. Results suggested that *S. aureus* bacterium produced proteinase and used the amino acids of cysteine-S-sulfonated keratin as nutrients. Additionally, the negatively charged structure of cysteine-S-sulfonated keratin exponentially improved the growth of the bacterium, in agreement with previous studies reported in the literature [8].

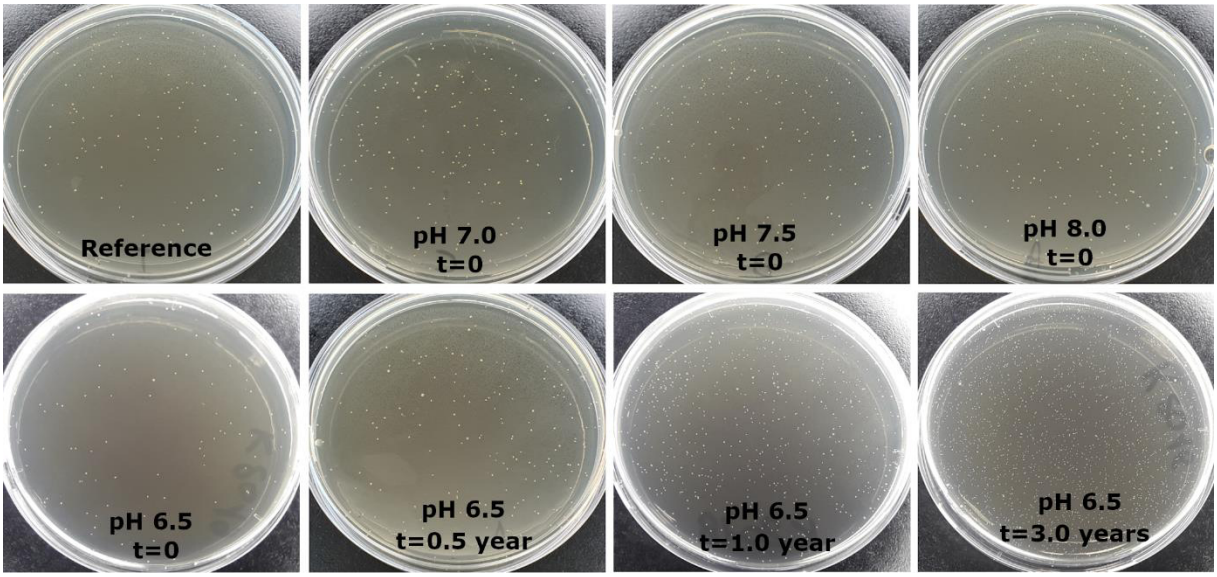

Figure 7. Antibacterial tests. Upper row: variation of pH; lower row: ageing of keratin.

It is thought that cysteine-S-sulfonated keratin does not have biocidal activity and that requires antimicrobial agents to obtain this property [79]. Nevertheless, cysteine-S-sulfonated keratin has demonstrated to be positively charged below pH ~5.25, giving rise to its biocidal activity. Moreover, this property is corroborated by the presence of ligands that create protein-ligand complexes, suitable for the application of cysteine-S-sulfonated keratin in drug delivery and wound healing as in the case of other proteins (albumin, zein and polylysine) [80,81]. All these results demonstrate that the biocidal activity of cysteine-S-sulfonated keratin can be modulated before dialysis by an accurate pH tuning. Finally, the antibacterial property of protonated cysteine-S-sulfonated keratin could contribute to reduce the use of antibiotics and to slow down the spread of methicillin-resistant *S. aureus* [82-84].

3.6. Cell viability on lyophilized cysteine-S-sulfonated keratin

The viability of hMSC at specific pH values is reported for selected samples – i.e., NaOH, HCl, citric acid and acetic acid titrations (Figure 8). In overall, results show a correlation between cell growth and the content of intramolecular β−sheet (Figure 2 and 3). In HCl case, it was noticed that the highest cell viability values were found where the percentage of intramolecular β−sheet was minimal and when the variations of β−sheet II structures were

also minimal. Meanwhile, the smallest cell viability values were found where the percentage of intramolecular β–sheet was maximal and when the percentage of β–sheet II was at its minimal value. Similar results were also observed for citric acid. In comparison with cysteine-S-sulfonated keratin without alkali or acid, a higher viability of hMSC was recognized in the case of NaOH. These results confirmed that the content of some secondary structures (i.e., intramolecular β–sheet) notably influence cell-material interaction, even overcoming the anti-adhesive effect of negatively charged proteins. Although, the microscopic interactions of selected ions (such as acetate, citrate, formate and bisulfite ions) with cells are not still completely understood, the proposed results confirm the positive contribution of bisulfite (pH 5.3 and 4.9) and citrate ions (pH 5.2) on cysteine-S-sulfonated keratin and hMSC interaction mechanisms - not detectable in the case of acetate ions (pH between 5.3 and 3.8). Furthermore, it is important to remember that in the literature cysteine-S-sulfonated keratin has also demonstrated its potential to promote fibroblast adhesion/growth, to act as a drug delivery system and to be a cytocompatible protein [85]. As a result, protonated cysteine-S-sulfonated keratin could be used to treat burn wounds as it promotes the proliferation of hMSC and offers protection against bacterial infections (specifically, *S. aureus*).

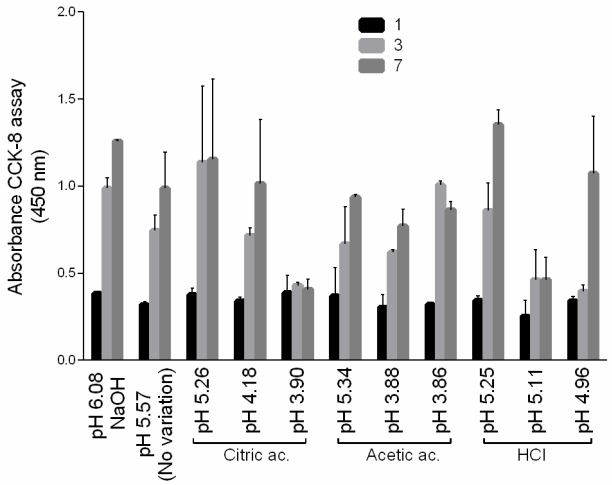

Figure 8. hMSC viability on cysteine-S-sulfonated keratin discs after different treatments.

4. Conclusion

The results demonstrated the importance of pH during the processing of cysteine-S-sulfonated keratin extracted by sulfitolysis, as it influences the biocidal activity, thermostability and *in vitro* cell-material interactions. Cysteine-S-sulfonated keratin in aqueous solutions showed its capacity to act like a protein buffer system, such as plasma proteins or hemoglobin. The protonation of side-chains and the presence of anionic ligands (i.e., citrate, formate, acetate and bisulfite ions) contributed to the formation of cysteine-S-sulfonated keratin-ligand complexes that alter the content of secondary structures. Additionally, the presence of anionic ligands also contributes to stabilize the biocidal activity of protonated cysteine-S-sulfonated keratin even in buffer solutions. Despite the fact that protonated cysteine-S-sulfonated keratin showed an excellent antibacterial activity, the same protein with negative charges increases exponentially the growth of *S. aureus*. As a result, the properties of cysteine-S-sulfonated keratin studied in this work turned out to be pH-switchable and these can be set up before dialysis, taking into account the presence of different ions in solution.

According to the reported experimental evidence, cysteine-S-sulfonated keratin could be successfully envisaged as hydrogels for cell culture, scaffolds for wound healing and capsules for drug delivery.

CRediT authorship contribution statement.

All authors participated in the design of the study, contributed to the writing of the paper, gave final approval for publication and agreed to be accountable for the work performed herein.

Declaration of Competing Interest.

The authors declare that they have no known competing financial interests or personal relationships that could have appeared to influence the work reported in this paper.

Acknowledgments. This research did not receive any specific grant from funding agencies in the public, commercial, or not-for-profit sectors.

Appendix A. Supplementary data. Supplementary data to this article can be found online at

References

[1] Ishihara M, Kishimoto S, Nakamura S, Sato Y, Hattori H. 2019 Polyelectrolyte complexes of natural polymers and their biomedical application. *Polymers* **11**, 672. (doi: 10.3390/polym11040672)

[2] Liu G. 2019 Tuning the properties of charged polymers at the solid/liquid interface with ions. *Langmuir* **35**, 3232-3247. (doi: 10.1021/acs.langmuir.8b01158)

[3] Basak Kaytmazer A, Seeman D, Baykal Minsky B, Dubin PL, Xu Y. 2013 Protein-polyelectrolyte interactions. *Soft Matter* **9**, 2553-2583. (doi: 10.1039/C2SM27002A)

[4] Dakhara SL, Anajwala CC. 2010 Polyelectrolyte complex: a pharmaceutical review. *Syst. Rev. Pharm.* **1**, 121-127. (doi: 10.4103/0975-8453.75046)

[5] Budd PM. 1996 Polyelectrolytes. In:. Allen G, Bevington JC (eds) Comprehensive Polymer Science and Supplements. Elsevier, pp 215-230. (doi: 10.1016/B978-0-08-096701-1.00011-2)

[6] Jayasuriya AC. 2017 Production of micro- and nanoscale chitosan particles for biomedical applications. In: Amber Jennings J, Bumgardner JD (eds) Chitosan Based Biomaterials Volume 1. Elsevier, pp 185-209. (doi: 10.1016/B978-0-08-100230-8.00008-X)

[7] Lee JH, Jung HW, Kang IK, Lee HB. 1994 Cell behaviour on polymer surfaces with different functional groups. *Biomaterials* **15**, 705-711. (doi: 10.1016/0142-9612(94)90169-4)

[8] Gottenbos B, Grijpma DW, Van der Mei HC, Feijen J, Busscher HJ. 2001 Antimicrobial effects of positively charged surfaces on adhering gram-positive and gram-negative bacteria. *J. Antimicrob. Chemother.* **48**, 7-13. (doi: 10.1093/jac/48.1.7)

[9] Cruz-Maya I, Guarino V, Almaguer-Flores A, Alvarez-Perez MA, Varesano A, Vineis C. 2019 Highly polydisperse keratin rich nanofibers: Scaffold design and *in vitro* characterization. *J. Biomed. Mater. Res. A* **107**, 1803-1813. (doi: 10.1002/jbm.a.36699).

[10] Shah A, Tyagi S, Naresh Bharagava R, Belhaj D, Kumar A, Saxena G, Dattatraya Saratale G, Mulla SI. 2019 Keratin production and its applications: current and future perstpetive. In: Sharman S,. Kumar A (eds) Keratin as a protein biopolymer. Springer, Cham, pp 19-35. (doi: 10.1007/978-3-030-02901-2_2)

[11] Aluigi A, Tonetti C, Vineis C, Tonin C, Mazzuchetti G. 2011 Adsorption of copper (II) ions by keratin/PA6 blend nanofibres. *Eur. Polym. J.* **47**, 1756-1764. (doi: :10.1016/j.eurpolymj.2011.06.009)

[12] Aluigi A, Rombaldoni F, Tonetti C, Jannoke L. 2014 Study of methylene blue adsorption on keratin nanofibrous membranes. *J. Hazard. Mater.* **268**, 156-165. (doi: 10.1016/j.jhazmat.2014.01.012)

[13] Figoli A, Ursino C, Sanchez Ramirez DO, Carletto RA, Tonetti C, Varesano A, De Santo MP, Cassano A, Vineis C. 2019 Fabrication of electrospun keratin nanofiber membranes for air and water treatment. *Polym. Eng. Sci.* 59, 1472-1478. (doi: 10.1002/pen.25146)

[14] Varesano A, Vineis C, Tonetti C, Sanchez Ramirez DO, Mazzuchetti G, Ortelli S, Blosi M, Costa AL. 2015 Multifunctional hybrid nanocomposite nanofibers produced by colloid electrospinning from water solutions. *Curr. Nanosci.* **11**, 41-48. (doi: 10.2174/1573413710666140922225056)

[15] Varesano A, Vineis C, Tonetti C, Sanchez Ramirez DO, Mazzuchetti G. 2014 Chemical and physical modifications of electrospun keratin nanofibers induced by heating treatments. *J. Appl. Polym. Sci.* **131,** 40532. (doi: 10.1002/app.40532)

[16] Paton LN, Gerrard JA,. Bryson WG. 2008 Two-dimensional gel electrophoresis of wool intermediate filament proteins. *J. Proteomics* **71**, 439-447. (doi: 10.1016/j.jprot.2008.06.008)

[17] Herbert BR, Molloy MP, Yan JX, Gooley AA, Bryson WG, Williams KL. 1997 Characterisation of wool intermediate filaments proteins separated by micropreparative two-dimensional electrophoresis. *Electrophoresis* **18**, 568-572. (doi: 10.1002/elps.1150180339)

[18] Plowman JE, Bryson WG, Flanagan LM, William Jordan T. 2002 Problems associated with the identification of proteins in homologous families: the wool keratin family as a case study. *Anal. Biochem.* **300**, 221-229. (doi: 10.1006/abio.2001.5459)

[19] Peralta Ramos ML, González JA, Fabian L, Pérez CJ, Villanueva ME, Copello GJ. 2017 Sustainable and smart keratin hydrogel with pH-sensitive swelling and enhanced mechanical properties. *Mater. Sci. Eng. C* **78**, 619-626. (doi: 10.1016/j.msec.2017.04.120)

[20] Galaburri G, Peralta Ramos ML, Lázaro-Martínez JM, Fernández de Luis R, Arriortua MI, Villanueva ME, Copello GJ. 2019 pH and ion-selective swelling behaviour of keratin and keratose 3D hydrogels. *Eur. Polym. J.* **118**, 1-9. (doi: 10.1016/j.eurpolymj.2019.05.043)

[21] Chen M, Ren X, Dong L, Li X, Cheng H. 2021 Preparation of dynamic covalently crosslinking keratin hydrogels based on thiol/disulfide bonds exchange strategy. *Int. J. Biol. Macromol.* **182**, 1259-1267. (doi: 10.1016/j.ijbiomac.2021.05.057)

[22] Li Y, Lin J, Zhi X, Li P, Jiang X, Yuan J. 2018 Triple stimuli-responsive keratin nanoparticles as carriers for drug and potential nitric oxide release. *Mater. Sci. Eng. C* **91**, 606-614. (doi: 10.1016/j.msec.2018.05.073)

[23] Liu P, Wu Q, Li Y, Li P, Yuan J, Meng X, Xiao Y. 2019 DOX-conjugated keratin nanoparticles for pH-sensitive drug delivery. *Colloids Surf. B* **181**, 1012-1028. (doi: 10.1016/j.colsurfb.2019.06.057)

[24] Zhang HF, Ma L, Su F, Ma XF, Li T, Jian-Zha-Xi W, Zhao GH, Wu ZM, Hou CL, Yan HJ. 2021 pH and reduction dual-responsive feather keratin – sodium alginate nanogels with high drug loading capacity for tumor-targeting DOX delivery. *Polym. Test.* **103**, 107375. (doi: 10.1016/j.polymertesting.2021.107375)

[25] European Food Safety Authority (EFSA), Antimicrobial resistance. https://www.efsa.europa.eu/en/topics/topic/antimicrobial-resistance (accessed 23 January 2022).

[26] National Health Service – England (NHS), Antibiotic resistance. https://www.nhs.uk/conditions/antibiotics/antibiotic-antimicrobial-resistance/ (accessed 23 January 2022).

[27] Kundukad B, Udayakumar G, Grela E, Kaur D, Rice SA, Kjelleberg S, Doyle PS. 2020 Weak acids as an alternative anti-microbial therapy. *Biofilm* **2**, 100019. (doi: 10.1016/j.bioflm.2020.100019)

[28] Van de Weert M, Haris PI, Hennink WE, Crommelin DJA. 2001 Fourier transform infrared spectrometric analysis of protein conformation: effect of sampling method and stress factors. *Anal. Biochem.* **297**, 160-169. (doi: 10.1006/abio.2001.5337)

[29] Cobb JS, Zai-Rose V, Correia JJ, Janorkar AV. 2020 FT-IR spectroscopic analysis of the secondary structures present during the desiccation induced aggregation of elastin-like polypeptide on silica. *ACS Omega* **5**, 8403-8413. (doi: 10.1021/acsomega.0c00271)

[30] Troullier A, Reinstädler D, Dupont Y, Naumann D, Forge V. 2000 Transient non-native secondary structures during the refolding of α-lactalbumin detected by infrared spectroscopy. *Nat. Struct. Biol.* **7**, 78-86. (doi: 10.1038/71286)

[31] Tian F, Russell Middaugh C, Offerdahl T, Munson E, Sane S, Howard R. 2007 Spectroscopic evaluation of the stabilization of humanized monoclonal antibodies in amino acid formulations. *Int. J. Pharm.* **335,** 20-31. (doi: 10.1016/j.ijpharm.2006.10.037)

[32] Baird G, Farrel C, Cheung J, Semple A, Blue J, Ahl PL. 2020 FTIR spectroscopy detects intermolecular beta-sheet formation above the high temperature Tm for two monoclonal antibodies. *Protein J.* **39**, 318-327. (doi: 10.1007/s10930-020-09907-y)

[33] Belton DJ, Plowright R, Kaplan D, Perry CC. 2018 A robust spectroscopic method for the determination of protein conformational composition – Application to the annealing of silk. *Acta Biomater.* **73**, 335-364. (doi: 10.1016/j.actbio.2018.03.058)

[34] DeFlores LP, Ganim Z, Nicodemus RA, Tokmakoff A. 2009 Amide I'—II′ 2D IR spectroscopy provides enhanced protein secondary structural sensitivity. *J. Am. Chem. Soc.* **131**, 3385-3391. (doi: 10.1021/ja8094922)

[35] Cardamone JM. 2010 Investigating the microstructure of keratin extracted from wool: peptide sequence (MALDI-TOF/TOF) and protein conformation (FTIR). *J. Mol. Struct.* **969,** 97-105. (doi: 10.1016/j.molstruc.2010.01.048)

[36] Litvinov RI, Faizulin DA, Zuev YF, Weisel JW. 2012 The α-helix to β-sheet transition in stretched and compressed hydrated fibrin clots. *Biophys. J.* **103**, 1020-2017. (doi: 10.1016/j.bpj.2012.07.046)

[37] Secundo F, Guerrieri N. 2005 ATR-FT/IR study on the interactions between gliadins and dextrin and their effects on protein secondary structure. *J. Agric. Food Chem.* **53**, 1757-1764. (doi: 10.1021/jf049061x)

[38] Wang C, Chen Z, Hong X, Ning F, Liu H, Zang J, Yan X, Kemp J, Musselman CA, Kutateladze TG, Zhao R, Jiang C, Zhang G. 2014 The structural basis of urea-induced protein unfolding in β-catenin. *Acta Crystallogr. Sect D: Biol. Crystallogr.* **D70**, 2840-2847. (doi: 10.1107/S1399004714018094)

[39] Houen G. 1996 The solubility of proteins in organic solvents. *Acta Chem. Scand.* **50**, 68-70. (doi: 10.3891/acta.chem.scand.50-0068)

[40] Bolton GR, Boesch AW, Basha J, LaCasse DP. 2011 Effect of protein and solution properties on the Donnan effect during the ultrafiltration of proteins. *Biotechnol. Prog.* **27**, 140-152. (doi: 10.1002/btpr.523)

[41] Sperelakis N. 2012 Gibbs-Donnan equilibrium potentials. In: Sperelakis N (eds) Cell Physiology Source Book (Fourth Edition). Elsevier, pp 147-151. (doi: 10.1016/B978-0-12-387738-3.00010-X)

[42] Mapleson W. 1987 Computation of the effect of Donnan equilibrium on pH in equilibrium dialysis. *J. Pharmacol. Methods* **17**, 231-242. (doi: 10.1016/0160-5402(87)90053-2)

[43] Costantino HR, Griebenow K, Langer R, Klibanov AM. 1997 On the pH memory of lyophilized compounds containing protein functional groups. *Biotechnol. Bioeng.* **53**, 345-348. (doi: 10.1002/(SICI)1097-0290(19970205)53:3<345::AID-BIT14>3.0.CO;2-J)

[44] Vakos HT, Kaplan H, Black B, Dawson B, Hefford A. 2000 Use of pH memory effect in lyophilized proteins to achieve preferential methylation of α-amino groups. *J. Protein Chem.* **19**, 231-237. (doi: 10.1023/A:1007064021743)

[45] Sanchez Ramirez DO, Carletto RA, Tonetti C, Truffa Giachet F, Varesano A, Vineis C. 2017 Wool keratin film plasticized by citric acid for food packaging. *Food Packaging and Shelf Life* **12**, 100-106. (doi: 10.1016/j.fpsl.2017.04.004)

[46] Sanchez Ramirez DO, Cruz-Maya I, Vineis C, Guarino V, Tonetti C, Varesano A. 2021 Wool keratin-based nanofibres – *In vitro* validation. *Bioengineering* **8**, 224. (doi: 10.3390/bioengineering8120224)

[47] Barth A, Zscherp C. 2002 What vibrations tell us about proteins. *Q. Rev. Biophys.* **35**, 369-430. (doi: 10.1017/S0033583502003815)

[48] Hellwing P, Rost B, Kaiser U, Ostermeier C, Michel H, Mäntele W. 1996 Carboxyl group protonation upon reduction of the *Paracoccus Denitrificans* cytochrome *c* oxidase: direct evidence by FTIR spectroscopy. *FEBS Lett.* **385**, 53-57. (doi: 10.1016/0014-5793(96)00342-0)

[49] Suzuki D, Sudo Y, Furutani Y, Takahashi H, Homma M, Kandori H. 2008 Structural changes of *Salinibacter* sensory Rhodopsin I upon formation of the K and M photointermediates. *Biochemistry* **47**, 12750-12759. (doi: 10.1021/bi801358b)

[50] Ricciardi V, Portaccio M, Manti L, Lepore M. 2020 An FTIR microspectroscopy ratiometric approach for monitoring X-ray irradiation effects on SH-SY5Y human neuroblastoma cells. *Appl. Sci.* **10,** 2974. (doi: 10.3390/app10082974)

[51] Townsend TM, Allanic A, Noonan C, Sodeau JR. 2012 Characterization of sulfurous acid, sulfite, and bisulfite aerosol systems. *J. Phys. Chem. A* **116**, 4035-4046. (doi: 10.1021/jp212120h)

[52] Risberg ED, Eriksson L, Mink J, Pettersson LGM, Skripkin MY, Sandström M. 2007 Sulfur X-ray adsorption and vibrational spectroscopic study of sulfur dioxide, sulfite, and sulfonate solutions and of the substituted sulfonate ions X3CSO3$^-$ (X = H, Cl, F). *Inorg. Chem.* **46,** 8332-8348. (doi: 10.1021/ic062440i)

[53] Jackson M, Mantsch HH. 1995 The use and misuse of FTIR spectroscopy in the determination of protein structure. *Crit. Rev. Biochem. Mol. Biol.* **30**, 95-120. (doi: 10.3109/10409239509085140)

[54] Cai S, Singh R. 2004 A distinct utility of the amide III infrared band for secondary structure estimation of aqueous protein solutions using partial least squares methods. *Biochemistry* **43**, 2541-2549. (doi: 10.1021/bi030149y)

[55] Bandekar J, Krimm S. 1979 Vibrational analysis of peptides, polypeptides, and proteins: characteristic amide bands of β-turns. *Proc. Natl. Acad. Sci. U.S.A.* **76**, 774-777. (doi: 10.1073/pnas.76.2.774)

[56] Barth A. 2007 Infrared spectroscopy of proteins. *Biochim. Biophys. Acta Bioenerg.* **1769**, 1073-1101. (doi: 10.1016/j.bbabio.2007.06.004)

[57] Klebe G. 2009 The foundations of protein-ligan interaction. In: Sussman JL, Spadon P (eds) From Molecules to Medicines – NATO Science for Peace and Security Series A: Chemistry and Biology. Springer, Dordrecht, pp 79-101. (doi: 10.1007/978-90-481-2339-1_6)

[58] Cao J. 1999 Melting study of the α-form crystallites in human hair keratin by DSC. *Thermochim. Acta* **335**, 5-9. (doi: 10.1016/S0040-6031(99)00055-6)

[59] Cao J, Joko K, Cook JR. 1997 DSC studies of the melting behavior of α-form crystallites in wool keratin. *Text. Res. J.* **67**, 117-123. (doi: 10.1177/004051759706700207)

[60] Istrate D, Popescu C, Er Rafik M, Möller M. 2013 The effect of pH on the thermal stability of fibrous hard α-keratins. *Polym. Degrad. Stab.* **98**, 542-549. (doi: 10.1016/j.polymdegradstab.2012.12.001)

[61] Istrate D, Er Rafik M, Popescu C, Demco DE, Tsarkova L, Wortmann FJ. 2016 Keratin made micro-tubes: the paradoxical thermal behavior of cortex and cuticle. *Int. J. Biol. Macromol.* **89**, 592-598. (doi: 10.1016/j.ijbiomac.2016.05.035)

[62] Brebu M, Spiridon I. 2011 Thermal degradation of keratin waste. *J. Anal. Appl. Pyrolysis* **91**, 288-295. (doi: 10.1016/j.jaap.2011.03.003)

[63] Bier JM, Verbeek CJR, Lay MC. 2014 Thermal transitions and structural relaxations in protein-based thermoplastics. *Macromol. Mater. Eng.* **299**, 524-539. (doi: 10.1002/mame.201300248)

[64] Balani K, Verma V, Agarwal A, Narayan R. 2015 Physical, thermal, and mechanical properties of polymers. In: Balani K, Verma V, Agarwal A, Narayan R (eds) Biosurfaces: A materials science and engineering perspective. John Wiley & Sons, New Jersey, pp. 329-344. (doi: 10.1002/9781118950623)

[65] Celej MS, Dassie SA, Freire E, Bianconi ML, Fidelio GD. 2005 Ligand-induced thermostability in proteins: thermodynamic analysis of ANS-albumin interaction. *Biochim. Biophy. Acta Proteins Proteomics* **1750**, 122-133. (doi: 10.1016/j.bbapap.2005.05.003)

[66] Celej MS, Montich GG, Fidelio GD. 2003 Protein stability induced by ligand binding correlates with changes in protein flexibility. *Protein Sci.* **12**, 1496-1506. (doi: 10.1110/ps.0240003)

[67] Pardhi DM, Şen Karaman D, Timonen J, Wu W, Zhang Q, Satija S, Mehta M, Charbe N, McCarron PA, Tambuwala M, Bakshi HA, Negi P, Aljabali AA, Dua K, Chellappan DK, Behera A, Pathak K, Watharkar RB, Rautio J, Rosenholm JM. 2020 Anti-bacterial activity of inorganic nanomaterials and their antimicrobial peptide conjugates against resistant and non-resistant pathogens. *Int. J. Pharm.* **587,** 119531. (doi: 10.1016/j.ijpharm.2020.119531)

[68] Neta P, Huie RE. 1985 Free-Radical Chemistry of Sulfite. *Environ. Health Perspect.* **64**, 209-2017. (doi: 10.1289/ehp.8564209)

[69] Betts RH, Voss RH. 1970 The Kinetics of Oxygen Exchange Between the Sulfite Ion and Water. *Can. J. Chem.* **48**, 2035-2041. (doi: 10.1139/v70-339)

[70] Goldberg RN, Parker VB. 1985 Thermodynamics of Solutions of $SO_{2(g)}$ in Water and of Aqueous Sulfur Dioxide Solution. *J. Res. Natl. Bur. Stand.* **90**, 341-358. (doi: 10.6028/jres.090.024)

[71] Howe PA, Worobo R, Sacks GL. 2018 Conventional measurements of sulfur dioxide (SO_2) in red wine overestimate SO_2 antimicrobial activity. *Am. J. Enol. Vitic.* **69**, 210-220. (doi: 10.5344/ajev.2018.17037)

[72] Tucker G. 2016 Pasteurization: principles and applications. In: Caballero B, Finglas PM, Toldrá F (eds) Encyclopedia of Food and Health. Elsevier, Oxford, pp. 264-269 (doi: 10.1016/B978-0-12-384947-2.00525-0)

[73] Bush RK, Taylor SL. 2014 Reactions to food and drug additives. In: Adkinson NF, Bochner BS, Burks AW, Busse WW, Holgate ST, Lemaske RF, O'Hehi' RE (eds) Middleton's Allergy Principles and Practice. Elsevier, Philadelphia, pp. 1340-1356. (doi: 10.1016/B978-0-323-08593-9.00083-8)

[74] Zhou C, Fey PD. 2020 The acid response network of *Staphylococcus aureus*. *Current Opinion in Microbiology* **55**, 67-73. (doi: 10.1016/j.mib.2020.03.006)

[75] Halstead FD, Rauf M, Moiemen NS, Bamford A, Wearn CM, Fraise AP, Lund PA, Oppenheim BA, Webber MA. 2015 The antibacterial activity of acetic acid against biofilm-producing pathogens of relevance to burns patients. *PLoS ONE* **10**, e0136190. (doi: 10.1371/journal.pone.0136190)

[76] Du X, Li Y, Xia YL, Ai SM, Liang J, Sang P, Ji XL, Liu SQ. 2016 Insights into protein-ligand interactions: mechanisms, models, and methods. *Int. J. Mol. Sci.* **17**, 144. (doi: 10.3390/ijms17020144)

[77] Jarvis AW, Lawrence RC. 1971 Production of extracellular enzymes and enterotoxins A, B, and C by *Staphylococcus Aureus*. *Infect. Immun.* **4**, 110-115. (doi: 10.1128/iai.4.2.110-115.1971)

[78] Shaw L, Golonka E, Potempa J, Foster SJ. 2004 The role and regulation of the extracellular proteases of *Staphylococcus Aureus*. *Microbiology* **150**, 217-228. (doi: 10.1099/mic.0.26634-0)

[79] Muñoz-Bonilla A, Echeverria C, Sonseca Á, Arrieta MP, Fernández-Garcia M. 2019 Bio-based polymers with antimicrobial properties towards sustainable development. *Materials* **12**, 641. (doi: 10.3390/ma12040641)

[80] Tarhini M, Pizzoccaro A, Benlyamani I, Rebaud C, Greige-Gerges H, Fessi H, Elaissari A, Bentaher A. 2020 Human serum albumin nanoparticles as nanovector carriers for proteins: application to the antibacterial proteins “neutrophil elastase” and “secretory leukocyte protease inhibitor”. *Int. J. Pharm.* **579**, 119150. (doi: 10.1016/j.ijpharm.2020.119150)

[81] Silva D, de Sousa HC, Gil MH, Santos LF, Martins Moutinho G, Serro AP, Saramago B. 2018 Antibacterial layer-by-layer coating to control drug release from soft contact lenses material. *Int. J. Pharm.* **553**, 186-200. (doi: 10.1016/j.ijpharm.2018.10.041)

[82] European Food Safety Authority (EFSA), Meticillin-resistant Staphyloccus aureus (MRSA). https://www.efsa.europa.eu/en/topics/topic/meticillin-resistant-staphylococcus-aureus-mrsa (accessed 23 January 2022)

[83] Centers for Disease Control and Prevention (CDC) – U.S. Department of Health & Human Services, Methicillin-resistant Staphylococcus aureus (MRSA). https://www.cdc.gov/mrsa/index.html (accessed 23 January 2022)

[84] National Health Service – England (NHS), MRSA. https://www.nhs.uk/conditions/mrsa/ (accessed 23 January 2022)

[85] Posati T, Giuri D, Nocchetti M, Sagnella A, Gariboldi M, Ferroni C, Sotgiu G, Varchi G, Zamboni R, Aluigi A. 2018 Keratin-hydrotalcites hybrid films for drug delivery applications. *Eur. Polym. J.* **105**, 177-185. (doi: 10.1016/j.eurpolymj.2018.05.030)